Pergamon

0301-9322(95)00009-7

Int. J. Multiphase Flow Vol. 21, No. 5, pp. 787–800, 1995

0301-9322/95 $9.50 + 0.00

OSMOPHORETIC MOTION OF DEFORMABLE PARTICLES

D. ZINEMANAS[1] and A. NIR[2]

[1]Department of Biomedical Engineering, Technion, Haifa 32000, Israel

[2]Department of Chemical Engineering, Technion, Haifa 32000, Israel

(Received 19 January 1994; in revised form 26 January 1995)

Abstract—Osmophoresis denotes the motion of cells or small capsules in concentration gradients. When a fluid particle encapsulated in a semi-permeable membrane is placed in a solution having non-uniform concentration the particle responds to the local osmotic differences. It may shrink or swell and it may move from its initial position depending on the external concentration field. The quasi-steady analysis of osmophoretic motion of a rigid spherical capsule in a constant gradient presented by Anderson is extended to consider the more realistic case in which the encapsulating membrane is deformable. The model considers the combined effects of local osmotic pressure difference and local normal stress component and integrates a simultaneous solution of the flow field and the surface deformation. We consider uniform and non-uniform concentration fields having zero and constant gradients, respectively. Various membrane properties and shapes and their influences are examined. In uniform concentrations the capsule goes through a single stage of adjustment of the shape to the developing concentration and stress differences. In fields with concentration gradients the solution indicates a three stage dynamics. A stage dominated by swelling, a stage of advance in the concentration field and a stage dominated by deformation during which the motion ceases. Osmophoresis of deformable particles appears to be a transient phenomenon.

Key Words: osmophoresis, capsules, deformable particles

INTRODUCTION

When a fluid particle surrounded by a semi-permeable membrane is immersed in a second solution in which a different concentration or a concentration gradient of the non-permeable solute exists, the osmotic flow through the membrane may cause it to move and deform. Gordon (1981) has proposed the term "osmophoresis" to describe this motion of a semi-permeable capsule in the presence of osmotic gradients and suggested that this mechanism may provide one possible explanation to the chemotactic motion of cells (Devreotes & Zigmond 1988) in response to concentration gradients of different solutes in the surrounding ambient fluid. Assuming that the osmotic force driving the solvent across the membrane represents the force that propels the cell, Gordon (1981) derived an expression for the osmophoretic velocity of a spherical particle by equating this propelling force to the Stokes viscous resistance exerted by the surrounding fluid on the cell. The velocity, thus calculated, was found to be proportional to the square of the particle size, to the external concentration gradient and inversely proportional to the viscosity of the surrounding fluid medium. Moreover, the cell was found to move toward regions of higher solute concentrations.

Pope (1982), inspired by Gordon's theory, tried to experimentally measure the force exerted on a semi-permeable membrane by an osmotic flow and found that the measured forces were not reproducible. The forces exhibited inconsistent directions and were much smaller in magnitude than those predicted by the theory. He concluded that solvent flux across the membrane may be a diffusion process, which does not transfer momentum to the membrane, rather than a viscous flow that exerts a drag on the membrane and that, thus, the osmophoretic velocities should usually be expected to be small.

Assuming that no mechanical force is exerted by the fluid on the membrane and that the fluid velocity through the membrane is proportional to the sum of the normal stresses and the osmotic pressure differences across it, Anderson (1983) solved the momentum and mass balances for the fluids and the solute for a rigid spherical vesicle, and obtained an expression for the osmophoretic velocity which was essentially different from that derived by Gordon. Anderson's osmophoretic velocity is indeed proportional to the concentration gradient but it is independent of the fluid viscosity and its dependence on the particle size is at most linear. More important, the particle is expected to move toward regions of lower rather than higher solute concentrations. The effects of

shape and permeability were also investigated (Anderson 1984) but no fundamental or qualitative differences were found regarding the particle motion in comparison with the spherical particle. In the limit of large diffusion rates, and low inner concentrations of the solute, the velocity for a spherical particle is found to be given by

$$\mathbf{v} = -\tfrac{1}{2} a L_p R T \nabla C_\infty \qquad [1]$$

where L_p is the membrane hydraulic conductivity, a is the particle radius, R and T denote the gas constant and the absolute temperature, respectively, and ∇C_∞ is the external undisturbed solute concentration gradient. For a non-spherical particle a similar expression is obtained including an additional shape and orientation factor. Thus, oblate or prolate spheroids with their symmetry axis parallel to the concentration gradient will move slower and faster, respectively, than a spherical cell (Anderson 1984).

Keh & Yang (1992) extended Anderson's analysis (1983) to examine the effects of the interaction between adjacent particles during osmophoretic motion. They found, for example, that two spherical particles aligned with the concentration gradient will move slower than a similar isolated particle. However, when the line of centers is normal to the concentration gradient the particles move faster than an isolated one in the same osmotic gradient.

Although Anderson's (1983, 1984) and Keh & Yang's (1992) theoretical analyses of the steady osmophoretic motion of particles has provided important basic understanding of the process, the analyses are limited to the study of the motion of rigid membranes that maintain their original shape and conserve the volume and initial concentrations of the encapsulated solution. Moreover, the possible effects of local and overall deformation as well as the development of tension gradients in the membrane were not considered. While, Anderson (1983) suggests that no qualitative difference between the motion of a rigid capsule and deformable particle are expected, no evaluation of the aforementioned effects was performed.

The main purpose of this communication is to examine the effects of the particle deformation and the development of membrane tensions on the osmophoretic motion. The analysis presented here follows the model of Anderson (1983, 1984) and extends it in order to incorporate these effects. The resulting unsteady osmophoretic dynamics accounts for the temporal volume and concentration changes due to swelling, for the external concentration changes due to the particle motion in the concentration gradient, for the local and total membrane deformations and for the development of normal and tangential stresses within the membrane. Since swelling is an important integral part of the dynamics of the osmophoretic motion and is interesting for itself (Zarda *et al.* 1977), the swelling of a non-spherical capsule in a constant external osmotic load was also studied. Pure swelling of a red blood cell was studied by Zarda *et al.* (1977) but their analysis is limited to inviscid particles where the membrane dynamics could not be evaluated. In this study the swelling process takes into account fluid viscosity and different membrane rheological properties, including those relevant to biological particles.

GOVERNING EQUATIONS

We consider an axisymmetric fluid particle composed of a viscous solution enveloped by a thin semi-permeable membrane, and freely suspended in an infinite stagnant viscous fluid in which different solute concentration as well as gradients of the concentration may exist. For mathematical simplicity both fluid solutions are assumed newtonian and incompressible with equal constant density, ρ, and viscosity, μ. The membrane is assumed to be completely impermeable to the molecules of the solute and the undisturbed concentration in the ambient solution is given by

$$C_\infty(\mathbf{x}) = C_\infty(\mathbf{x}_0) + \nabla C_\infty \cdot (\mathbf{x} - \mathbf{x}_0) \qquad |\mathbf{x}| \to \infty \qquad [2]$$

with a constant gradient, ∇C_∞, aligned with the particle axis of symmetry. It is also assumed that the diffusion of the solute is rapid compared to the convective transport.

In the absence of inertial effects, the inner and outer flow fields are governed by the Stokes equations with the stress, pressure and velocity, denoted by $\boldsymbol{\sigma}$, P and $\mathbf{v}$, respectively, defined in the usual manner. The velocity vanishes far from the particle and is continuous at the interface.

The jump in the surface tractions is equal to the interfacial force, **f**, i.e.

$$\Delta(\boldsymbol{\sigma} \cdot \mathbf{n}) = \mathbf{f} \qquad \mathbf{x} \in S \qquad [3]$$

where **n** is a normal unit vector oriented outward and Δ denotes the outer minus inner difference. The interfacial force is given by

$$\mathbf{f} = (\boldsymbol{\gamma} : \nabla \mathbf{n})\mathbf{n} + \nabla_s \cdot \boldsymbol{\gamma} \qquad [4]$$

Here $\boldsymbol{\gamma}$ denotes the interfacial stress tensor and $\nabla_s = (\mathbf{I} - \mathbf{nn}) \cdot \nabla$ is a gradient tangent to the surface. The first and second terms in the RHS of [4] are the interfacial normal and tangential tractions, respectively.

The stress tensor, $\boldsymbol{\gamma}$, depends on the particular rheology of the membrane and is generally expressed as a function of the strain tensor, **e**, or the stretch ratio, λ. The constitutive equation for a material representing the properties of a red blood cell membrane which is used in this study has been proposed by Skalak *et al.* (1973) and is of the form

$$\gamma_{11} = K'\left(\frac{\lambda_1^3}{\lambda_2} - 1\right) + K''(\lambda_1^2\lambda_2^2 - 1)\lambda_1\lambda_2 \qquad [5]$$

here K' and K'' are constants, γ_{11} is the stress in the 1 principal direction and the second principal stress has a similar form but with the 1 and 2 subscripts interchanged. The main rheological characteristic of this type of membrane is that it is highly resistant to area changes. The effect of these area changes on the stresses is represented by the second term in the RHS of [5] and depend quantitatively on the value of K''. In addition, a second type of membrane which does not conserve area and has linear elastic rheological characteristics, $\gamma_{ii} = Ke_{ii}$, where K is a constant and there is no summation on i, is considered. In both membrane models bending moments are neglected.

The membrane rate of strain is related to the membrane velocity by the expression (Waxman 1984)

$$\frac{\mathrm{De}}{\mathrm{D}t} = \frac{1}{2}(\nabla_s \mathbf{v}_s + \nabla_s \mathbf{v}_s^{\mathrm{T}}) - v_n \nabla \mathbf{n} \qquad [6]$$

which is used to follow the membrane deformations. Here $\mathbf{v}_s = (\mathbf{I} - \mathbf{nn}) \cdot \mathbf{v}$ is the membrane tangential velocity and $v_n = \mathbf{v} \cdot \mathbf{n}$ its normal component. The first RHS term in [6] denotes the rate of deformation due to the tangential motion while the second term describes the deformation due to the normal motion. The principal strains and the stretch ratio are related by $e_{ii} = 1/2(\lambda_i^2 - 1)$ (no summation on i).

The osmotic pressure and the stress field differences across the membrane induce a normal solvent osmotic velocity relative to the membrane as given by (Anderson 1983)

$$v_{os} = L_p[\Delta(\boldsymbol{\sigma} : \mathbf{nn}) + RT\Delta C] \qquad [7]$$

Note that the van't Hoff osmotic term is valid for low solute concentrations and that the normal stresses difference is used instead of the pressure difference, $-\Delta P$. This interchange follows an assumption by Anderson (1983). It is expected to be of no major significance and it also simplifies the numerical mathematical procedure since $\Delta(\boldsymbol{\sigma} : \mathbf{nn}) = \boldsymbol{\gamma} : \nabla \mathbf{n}$.

A solution of the equations of motion subject to the aforementioned boundary conditions for the interfacial velocity follows the analysis of Rallison & Acrivos (1978). When [7] is taken into account the motion of the membrane is given by

$$\mathbf{v}_m(\mathbf{x}) = -\frac{1}{8\pi\mu}\int_S \mathbf{J}(\mathbf{x} - \mathbf{y}) \cdot \mathbf{f}(\mathbf{y})\, \mathrm{d}S_y - v_{os}(\mathbf{x})\mathbf{n} \qquad \mathbf{x}, \mathbf{y} \in S \qquad [8]$$

where **J** is the single layer potential for the Stokes flow (Rallison & Acrivos 1978). The first term in the RHS of [8] is the contribution of the motion of the interface (membrane) due to the distribution of interfacial forces, **f**, while the second term represents the motion of the membrane relative to the fluid.

The quasi-steady evolution of the membrane location in the viscous field can thus be determined by the kinematic condition

$$\frac{\mathrm{D}\mathbf{R}(\mathbf{x})}{\mathrm{D}t} = \mathbf{v}_{\mathrm{m}} \qquad \mathbf{x} \in S \qquad [9]$$

where $\mathbf{R}(\mathbf{x})$ denotes the position of the interface S.

Finally, to calculate the osmophoretic velocity from [8] the solute concentration difference across the membrane must be simultaneously evaluated. In the limit of negligible convective mass transport effects, the conservation of solute requires that

$$\nabla^2 C = 0 \quad \mathbf{x} \in V, V' \qquad [10]$$

Here C denotes the solute concentration. Equation [10] is subject to the condition that a semi-permeable membrane does not allow solute flow through it

$$\nabla C \cdot \mathbf{n} = 0 \qquad \mathbf{x} \in S \qquad [11]$$

and that the solute concentration in V' approaches $C_\infty(\mathbf{x})$, given by [1], as $|\mathbf{x}| \to \infty$.

For the inner concentration field the solution of [10] implies a uniform concentration $C_{\mathrm{in}} = (C_{\mathrm{in0}} V_0)/V$, where C_{in0} and V_0 are the initial solute concentration and particle volume, respectively. Their product is, thus, the total amount of solute in the particle. The solution of the outer solute concentration for an arbitrary surface is given by a single layer potential

$$C(\mathbf{x}) = \int_S \frac{g(\mathbf{y})}{|\mathbf{x} - \mathbf{y}|} \mathrm{d}S_y \qquad \mathbf{y} \in S \qquad [12]$$

where the distribution $g(\mathbf{y})$ is given by the solution of

$$g(\mathbf{x}) = \frac{1}{2\pi} \nabla C_\infty \cdot \mathbf{n} + \int_S g(\mathbf{y}) \nabla\left(\frac{1}{|\mathbf{x} - \mathbf{y}|}\right) \cdot \mathbf{n} \, \mathrm{d}S_y \qquad \mathbf{x}, \mathbf{y} \in S \qquad [13]$$

For the case of regular ellipsoids the solution for the outer solute concentration on the particle surface is given by Anderson (1984). Approximations based on this solution for spheroidal particles can be employed.

The set of equations is rendered non-dimensional by choosing characteristic values for the different variables. Following Anderson (1983), and choosing an appropriate representative membrane tension value, γ_0, the characteristic values are

$$x = a, \quad v = L_{\mathrm{p}} RT \Delta C_0, \quad \sigma = \frac{\mu v}{a}, \quad C = \Delta C_0, \quad t = \frac{a}{v}, \quad \gamma = \gamma_0 \qquad [14]$$

where for non-spherical capsules a is defined using the volume, $a = (3V/4\pi)^{1/3}$. ΔC_0 is the relevant concentration magnitude, i.e. $\Delta C_0 = |C_\infty - C_{\mathrm{in0}}|$ for the case of swelling and $\Delta C_0 = |\nabla C_\infty| a$ for the case of osmophoretic motion. For a typical biological system the values of the physical parameters are: $a = 10^{-5}$ m, $C_\infty = 10^{-10}$ mol/m^3, $C_{\mathrm{in0}} = 2 \times 10^{-10}$ mol/m^3, $\mu = 10^{-3}$ N-s/m^2, $T = 300$ K, $L_{\mathrm{p}} = 10^{-11}$ m^3/N-s and $\nabla C_\infty = 10^{-11}$ mol/m^4. In addition, based on the values of the parameters $K' = 5 \times 10^{-6}$ N/m and $K'' = 10^{-1}$ N/m in [5], used by Zarda *et al.* (1977), $\gamma_0 = 1 \times 10^{-3}$ N/m is assumed, an intermediate value between K' and K''. For the linear elastic membrane γ_0 was chosen equal to K. Using these values and the definitions [14], [8], [3] and [7] we obtain the non-dimensional form

$$\mathbf{v}_{\mathrm{m}}(\mathbf{x}) = -\frac{\beta}{8\pi} \int_S \mathbf{J}(\mathbf{x} - \mathbf{y}) \cdot \mathbf{f}(\mathbf{y}) \, \mathrm{d}S_y - \mathbf{v}_{\mathrm{os}}(\mathbf{x}) \qquad \mathbf{x}, \mathbf{y} \in S \qquad [15]$$

$$\Delta(\boldsymbol{\sigma} \cdot \mathbf{n}) = \beta \mathbf{f} = \beta[(\boldsymbol{\gamma} : \nabla \mathbf{n})\mathbf{n} + \nabla_{\mathrm{s}} \cdot \boldsymbol{\gamma}] \qquad \mathbf{x} \in S \qquad [16]$$

$$v_{\mathrm{os}} = \delta(\boldsymbol{\gamma} : \nabla \mathbf{n}) + (C_{\mathrm{out}} - C_{\mathrm{in}}) \qquad [17]$$

where the dimensionless parameters δ and β are defined by

$$\delta = \frac{L_p \gamma_0}{av} = \frac{\gamma_0/a}{RT\Delta C} = \frac{\text{elastic pressure difference}}{\text{osmotic pressure difference}} \quad [18]$$

$$\beta = \frac{\gamma_0}{\mu v} = \frac{\text{elastic forces}}{\text{viscous forces}} \quad [19]$$

The first parameter denotes the ratio between the normal stress difference, due to the membrane tractions, and the osmotic pressure difference across the membrane while the second designates the ratio between elastic and viscous forces. Using the above typical data, the characteristic non-dimensional parameters are: $\delta = 4 \times 10^{-2}$ and $\beta = 4 \times 10^{5}$. Note that δ/β is the parameter $\mu Lp/a$ that appears in Anderson's (1983) analysis since, in the absence of interfacial tensions, it is the unique dimensionless parameter in the system.

NUMERICAL PROCEDURE

For arbitrary axisymmetrical particle shape and interfacial rheology properties, [15] needs to be solved numerically and in parallel with the evolution of the shape [9] and the interfacial deformations [6]. Evaluation of the membrane velocity from [15] is done using a numerical calculation of the surface integral appearing in the first RHS term of that equation. Since the kernel **J** is singular at $\mathbf{y} \rightarrow \mathbf{x}$ the integral is evaluated in two parts. At each surface point the asymptotic part of the singular kernel is subtracted from the integrand and is integrated analytically. The remaining regular integral is evaluated numerically and the two results are combined. The numerical details of the solution and a description of the mathematical algorithm were presented elsewhere (Zinemanas & Nir 1988, 1992) describing similar situations where the motion of a biological capsule is determined by active surface tractions. The procedure and an asymptotic evaluation validating the numerical accuracy are briefly described in the appendix. In the next section this algorithm is implemented in the study of the osmotic swelling and of the unsteady osmophoretic motion of particles with different shapes and membrane rheological properties. Spherical and various regular ellipsoidal initial shapes were chosen so that the present numerical results can be compared with previous calculations.

RESULTS AND DISCUSSION

In this section the evaluation of the swelling and osmophoretic motion of a particle is performed using the model described above and assuming that, in all cases, the membrane is initially in an unstressed state and with its symmetry axis aligned with the outer concentration gradient. The particle is subject to an average positive osmotic load, $C_{in} - C_{out}(\mathbf{x}_0) > 0$.

Osmotic swelling

The osmotic swelling of a particle is simulated by imposing a uniform solute concentration difference between the inner and outer solutions. An initial oblate (disk-like) shape is considered since it resembles the red blood cell profile and because such particles, during the swelling process, show volume changes as well as shape deformations in contrast to the case of a spherical shell where only a change of volume is expected with the shape remaining unaltered.

Figures 1 and 2 show the evolution of various particle variables under the effects of different initial osmotic loads, $C_{in} - C_{out}$, for a red blood cell membrane rheology, described by [5], and for an elastic rheology, respectively. It is noted that the two membrane rheologies show different deformation patterns. This is due to the different balance in each case between the volume increases imposed by the osmotic solvent inflow and the ability of the membrane to undergo area changes. These effects are clearly seen in figure 1(a)–(d) where the particle surface area, volume, aspect ratio and the inner concentration are depicted. It is observed that while the volume of the area conserving shell increases monotonically, the area, for small osmotic loads, initially increases but later returns to almost its initial value. Evidently, the compensation for the relative volume increase is realized by the overall deformation, demonstrated by the changes in the particle aspect ratio,

$D = 2R_{max}/(z_{max} - z_{min})$ [figure 1(c)]. At large osmotic loads, however, the large volume changes cannot be compensated only by shape deformation and the pressure differences that result from the membrane tension. The particle surface approaches a spherical shape and the surface area increases as well, until equilibrium conditions will ultimately be obtained when the osmotic difference is compensated by the inner to outer pressure difference which equals the normal membrane stresses. Evidently, since the amount of solute in the particle is constant, the concentration [figure 1(d)] is inversely proportional to the instantaneous volume.

The corresponding behavior of an elastic membrane which does not exhibit significant resistance to area changes is depicted in figure 2(a)–(d). In this case the surface area and the volume increase monotonically and the particle deforms considerably.

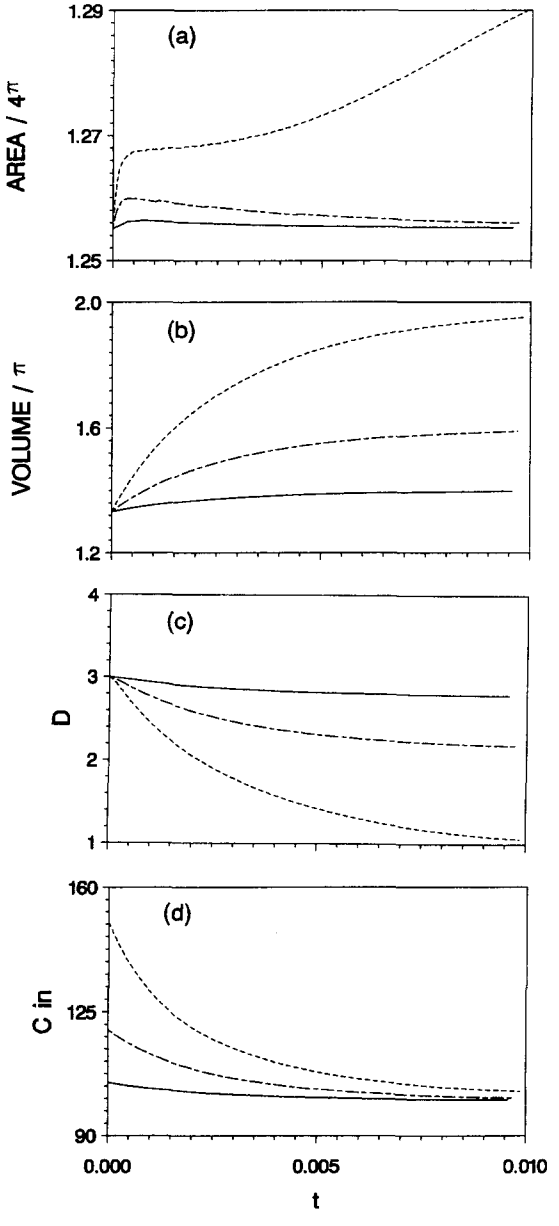

Figure 1. The dynamics of the swelling process of an oblate spheroid encapsulated in an area-conserving membrane in a positive osmotic load, $C_{in} - C_{out} > 0$ with $C_{out} = 100$. (a) Surface area, (b) volume, (c) spheroidal aspect ratio and (d) inner concentration. ——, – – – and – – – denote initial ΔC_0 equal to 5, 20 and 50, respectively. The corresponding values of δ are equal to 8×10^{-3}, 2×10^{-3} and 8×10^{-4}.

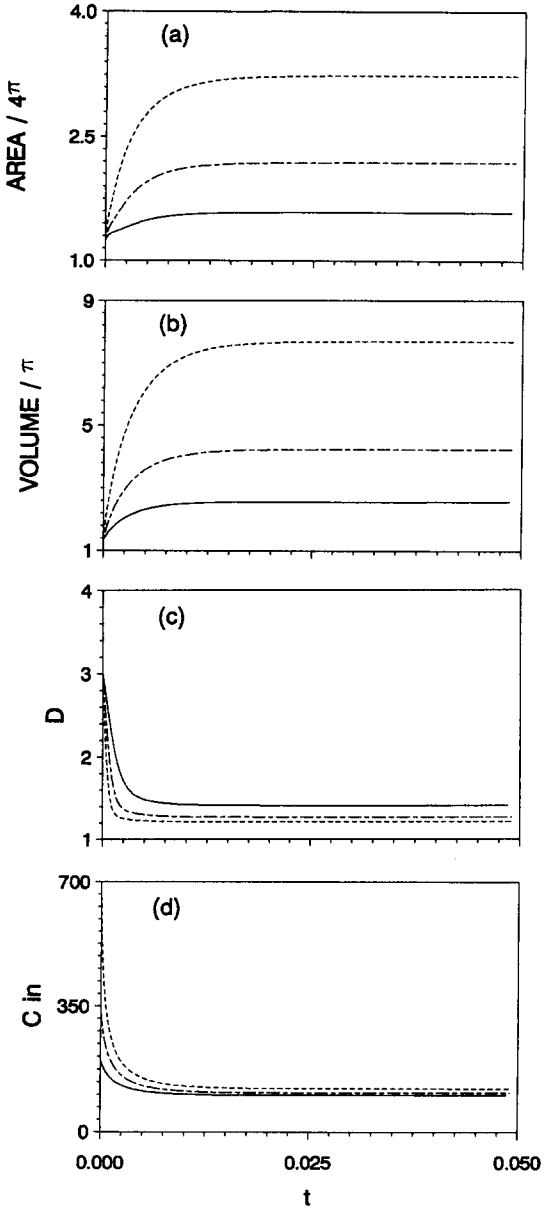

Figure 2. The dynamics of the swelling process of an oblate spheroid encapsulated in a linear elastic membrane in a positive osmotic load, $C_{in} - C_{out} > 0$ with $C_{out} = 100$. (a) Surface area, (b) volume, (c) spheroidal aspect ratio and (d) inner concentration. ——, – – – and – – – denote initial ΔC_0 equal to 200, 350 and 600, respectively. The corresponding values of δ are equal to 2×10^{-4}, 1.14×10^{-4} and 6.66×10^{-5}.

The general behavior of the osmotic swelling of a particle may be summarized by characterizing it in terms of the non-dimensional parameter δ. For large values of this parameter, i.e. large membrane tensile properties compared to the imposed osmotic pressures or relatively small osmotic loads, the local as well as the overall deformations are expected to be small since only small volume changes are required to induce membrane tensions large enough to balance the osmotic pressure difference or to cause the concentration difference to vanish. In the other limit, when $\delta \ll 1$, the osmotic pressure difference is balanced by large volume changes and local and overall deformations which reduce the inner solute concentration, thereby, reducing the osmotic load in addition to producing the membrane tensions necessary to oppose the osmotic difference. In the intermediate range of $\delta \sim O(1)$, as well as in the previous asymptotic cases, the particle deforms,

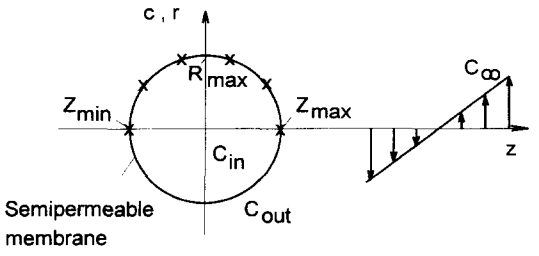

Figure 3. The underformed spherical capsule in the concentration gradient. Crosses indicate the initial location points where the axial velocities depicted in figure 4 are evaluated.

according to its membrane rheological properties, until the pressure and osmotic differences are balanced.

Osmophoretic motion

The first case considered is of a spherical particle encapsulated in a semi-permeable linear elastic membrane and placed in a linear solute concentration field [2] with its center at $\mathbf{x}_0$ (see figure 3). The initial osmotic load is positive yet small $C_{in} - C_{out} = 0.1$. Figure 4 shows the evolution of the axial velocity, under the conditions described, of 6 surface points initially distributed at equal distances along a meridional line from pole to pole. For comparison, the velocity as calculated by Anderson (1983) for a rigid spherical particle under quasi-steady conditions, is also shown. The corresponding simultaneous evolution of the particle surface area, volume, concentration and aspect ratio is depicted in figure 5(a)–(d). Clearly, three different stages are observed. The initial one corresponds to the swelling process during which surface area, volume and concentration changes are observed [figures 5(a)–(c)], but much smaller shape deformations are evident [figure 5(d)]. Simultaneously, membrane tensions and tension gradients develop in a characteristic non-dimensional time scale of the order of $1/\beta$. The second stage is characterized by a nearly constant axial velocity which corresponds to Anderson's rigid particle osmophoretic motion. During this stage, surface area, volume and concentration changes are almost negligible and shape deformations are still small.

In the third stage the motion of the particle is halted. This effect was not predicted for particles with a rigid membrane that cannot develop interfacial tension gradients (Anderson 1983). As can be observed in figures 4 and 5 the constant osmophoretic motion of a rigid particle continues even after the volume and surface area increased due to the swelling. Furthermore, the normal membrane tension component, $\gamma : \mathbf{Vn}$, is already developed considerably as is evident in figure 6. Yet these changes do not affect the osmophoretic velocity as long as they are not accompanied by shape defromations. The increase of the membrane tension is not sufficient to render the first term

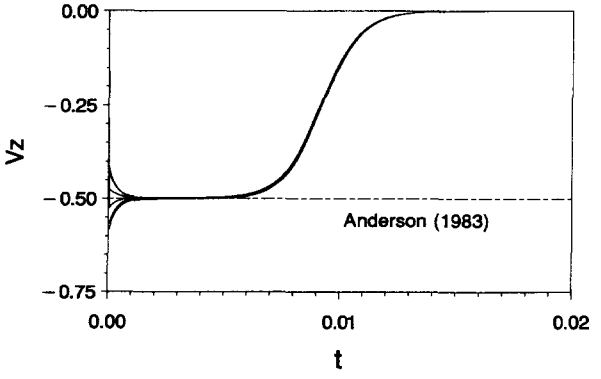

Figure 4. The evolution of the axial osmophoretic velocity, V_z, of an initially spherical capsule enveloped by a semi-permeable elastic membrane. The various lines correspond to six points located initially equidistantly on the surface along a meridional line.

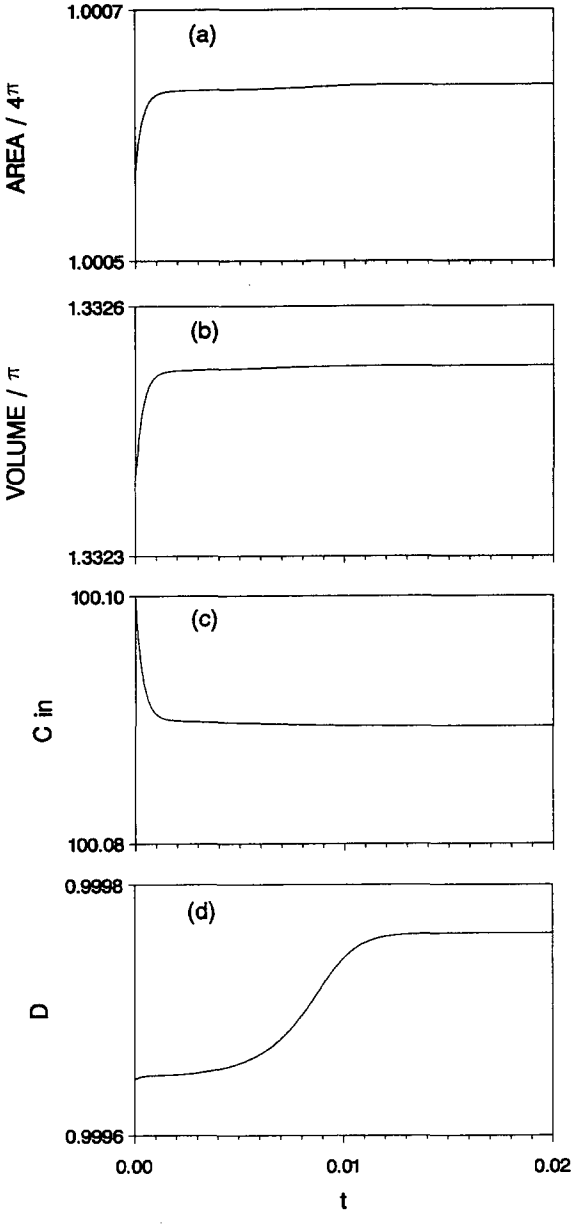

Figure 5. The dynamics of (a) the surface area, (b) the volume, (c) the inner concentration and (d) the aspect ratio during the osmophoresis of an initially spherical elastic semi-permeable membrane in a concentration gradient. $C_{in} - C_{out}(x_0) = 0.1$ initially.

on the RHS of [15] considerable enough to balance the osmotic velocity. However, when first order local deformations occur [see figure 5(d)] the resulting non-uniform interfacial force distribution produce a viscous motion that grows until it ultimately compensates the entire osmotic velocity. The time scale in which this change occurs depends on the membrane rheological properties and on the tension that developed in the swelling stage and prevails during the osmophoretic stage (figure 6) and is, non-dimensionally, of the $O(\gamma^{-1})$.

In figure 7 we compare the evolution of the three contributions to the mean velocities normal to the capsule surface, V_{mean}, defined by inward flux per unit capsule area. Among the components comprising the osmotic velocity ([17]) the normal component due to the osmotic pressure difference, $C_{out} - C_{in}$, is always dominant over that due to the normal stress difference (denoted by the first term on the RHS of [17]). The normal component of the newtonian viscous term due to the distribution of tension and shape changes (i.e. normal component of the first term on the RHS

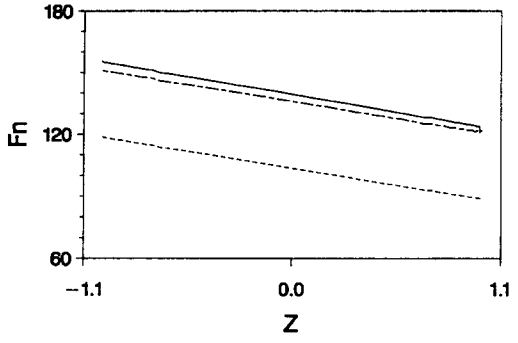

Figure 6. The distribution of non-dimensional membrane tensions, $\gamma : \nabla n$, along the axis of symmetry of an initially spherical elastic membrane during the osmophoresis process. – – –, – – – and —— denote tension distributions during the swelling, constant and halting stages, respectively, at $t = 0.0005$, 0.004 and 0.015.

of [15]) grows with the development of the deformation and tensions and ultimately balances the contribution of the osmotic load. Thus, as shown in figure 7, there is a net fluid flux into the capsule during the initial swelling and constant axial velocity stages referred to in the discussion of figure 5, and this flux diminishes as the motion stops.

The osmophoretic dynamics of non-spherical particles are not qualitatively different. The development of velocity for prolate and oblate spheroids with initially unstressed membranes, are shown in figures 8 and 9. Here again the three stages exist. In the first short one the swelling takes place and much of the inner concentration, volume and surface area changes occur. During the second stage of steady osmophoretic motion, deformation and tension gradients develop until the particle comes to a complete stop. The intermediate velocities correspond to Anderson's (1984) predictions for rigid spheroidal membranes.

Figure 10 depicts the effect of the variation of the surface mechanical properties on the osmophoretic motion of a spherical capsule. At a higher elastic coefficient, K, the capsule ceases to move in a shorter time. Since higher K results in a more rapid increase of the surface forces it is also expected that the total deformation at complete halt will be less developed. The behavior shown in the figure does not suggest that there exists a critical elastic modulus beyond which the capsule eventually comes to rest. The asymptotic value of the osmophoretic speed at the intermediate stage remains, however, unaltered.

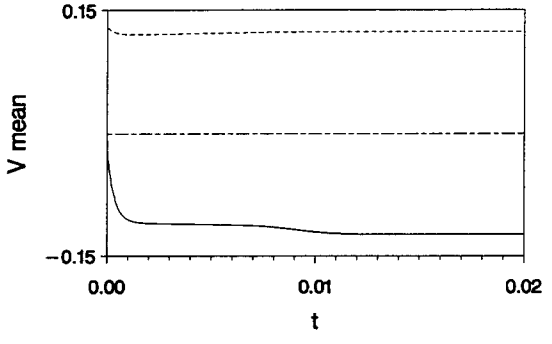

Figure 7. The contribution of various driving forces to the mean inward component, V_{mean}, of the osmophoretic velocity of an initially spherical capsule. —— denotes the newtonian viscous velocity and – · – and – – – correspond to the normal stress difference and the osmotic load components in the osmotic velocity, respectively.

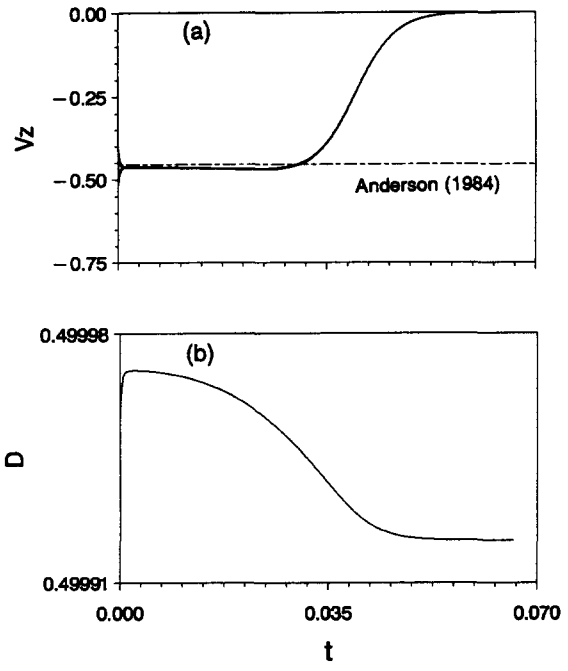

Figure 8. The evolution of the axial osmophoretic velocity and the aspect ratio of an initially prolate capsule enveloped by a semi-permeable elastic membrane. (a) Osmophoretic velocity and (b) aspect ratio.

CONCLUSIONS

The motion of particles in a concentration gradient is different for rigid particles and for particles with deformable membranes that can develop and transmit surface forces. In the first case a quasi-steady osmophoretic velocity is predicted. When surface tensions and local deformations are

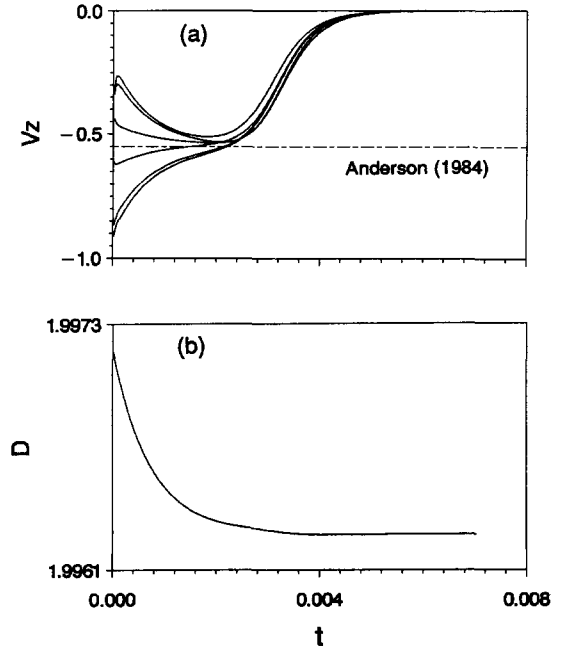

Figure 9. The evolution of the axial osmophoretic velocity and the aspect ratio of an initially oblate capsule enveloped by a semi-permeable elastic membrane. (a) Osmophoretic velocity and (b) aspect ratio.

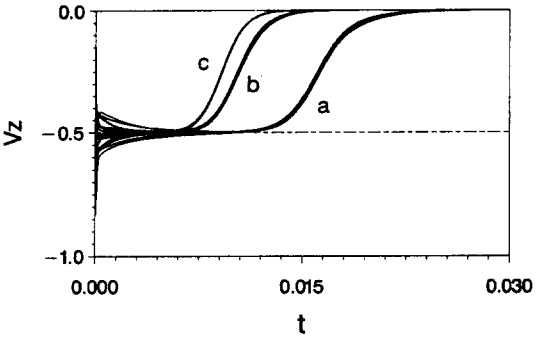

Figure 10. The evolution of the axial osmophoretic velocity, V_z, of initially spherical capsules enveloped by different semi-permeable elastic membranes. The various lines correspond to six points located initially equidistantly on the surface along a meridional line. (a) $K = 2 \times 10^{-4}$ ($\beta = 8 \times 10^4$), (b) $K = 1 \times 10^{-3}$ ($\beta = 4 \times 10^5$) and (c) $K = 5 \times 10^{-3}$ N/m ($\beta = 2 \times 10^6$).

incorporated in the analysis the particle motion is ultimately halted since the surface tractions eventually blance the osmotic load. Osmophoresis of deformable particles has a transient dynamics.

REFERENCES

Anderson J. L. 1983 Movement of a semipermeable vesicle through an osmotic gradient. *Phys. Fluids* **26,** 2871–2879.

Anderson J. L. 1984 Shape and permeability effects on osmiophoresis. *Phys. Chem. Hydrody.* **5,** 205–216.

Devreotes P. N. & Zigmund S. H. 1988 Chemotaxis in eukaryotic cells: a focus on leukocytes and dictyostelium. *Ann. Rev. Cell Bio.* **4,** 649–686.

Gordon L. G. M. 1981 Osmophoresis. *J. Phys. Chem.* **85,** 1753–1755.

Keh H. J. & Yang F. R. 1992 Particle interactions in osmophoresis. *Int. J. Multiphase Flow* **18,** 593–615.

Pope O. G. 1982 Investigation of osmophoresis. *J. Phys. Chem.* **86,** 1869–1870.

Rallison J. M. & Acrivos A. 1978 A numerical study of the deformation and burst of a viscous drop in general shear flows. *J. Fluid Mech.* **89,** 191–200.

Skalak R., Tozeren A., Zarda P. R. & Chien S. 1973 Strain energy function of red blood cell membranes. *Biophys. J.* **13,** 245–264.

Waxman A. M. 1984 Dynamics of a couple-stress fluid membrane. *Stud. Appl. Math.* **70,** 63–86.

Zarda P. R., Chien S. & Skalak 1977 Elastic deformations of red blood cells. *J. Biomech.* **10,** 211–221.

Zinemanas D. & Nir A. 1988 On the viscous deformation of biological cells under anisotropic surface tension. *J. Fluid Mech.* **193,** 217–241.

Zinemanas D. & Nir A 1992 A fluid-mechanical model of deformation during embryo exogastrulation. *J. Biomech.* **25,** 341–346.

APPENDIX

The quasi-stationary nature of the equations of motion allows a simple calculation scheme in which the surface velocities may be determined from the known instantaneous solute concentration and membrane shape and tensions. This velocity is employed in the kinematic conditions to evaluate by means of an updated lagrangian procedure, new shape, deformations and interfacial force profiles.

The spacial derivatives were evaluated using a finite-difference scheme. The contour of the axisymetric surface was divided into $M - 1$ intervals by distributing M points along a meridian line. Initially, these intervals were selected equal, however, any other arbitrary choice could have been used to anticipate crowding or separation of the material points under the effects of the surface motions and deformations. Since separation distances change as the points move, a finite-

difference scheme for unequal intervals was employed while second-order accuracy was maintained when evaluating first and second derivatives using three- and five-point algorithms.

In evaluating surface velocities it is noted that as $\mathbf{y} \rightarrow \mathbf{x}$ the axisymetric components of the kernel $\mathbf{J}$ in [15] possess a logarithmic singularity, except at the poles where this singularity is of $O(|\mathbf{x}-\mathbf{y}|^{1/2})$, and therefore the expression is integrable everywhere. Thus, to evaluate the velocity at a given point x_n, the leading orders of the singular kernels, up to $O(|\mathbf{x}-\mathbf{y}|^2)$, were subtracted from the integrand in the interval between x_{n-1} and x_{n+1}. The regular integration which resulted was calculated using Simpson's second-order method and added to the analytical integration of the asymptotic singular expansion between x_{n-1} and x_{n+1}. $M = 60$ was used in most cases as a compromise between numerical accuracy and limited computer resources.

Once the interfacial velocity was found, shape and interfacial tensions were computed for each material point on the surface by means of a straightforward Newtonian integration which, for the shape variations, becomes

$$\mathbf{R}(t + \mathrm{d}t) = \mathbf{R}(t) + \mathbf{v}(t)\Delta t \qquad [A1]$$

Since there is no obvious criterion for the stability of this quasi steady evolution of the shape, an arbitrary time increment Δt was chosen having the general form

$$\Delta t = C\frac{\min|\Delta \mathbf{x}|}{\max|\Delta \mathbf{v}|} \qquad [A2]$$

where $\Delta \mathbf{x}$ and $\Delta \mathbf{v}$ are the distance and velocity difference between two adjacent points. $C = 1 \times 10^{-7}$ was a typical value used as it was found sufficiently small to avoid interfacial instabilities which arise at larger time increments due to the membrane properties.

The validity of the numerical calculation can be established by comparing the results to calculations using an asymptotic analysis for the initial small deformations while the membrane tensions are not large. The equations of motion and the equations for the interfacial tensions were expanded by means of spherical harmonics and were solved for the case where a spherical capsule is embedded in a solution in which the undisturbed solute concentration and the capsule inner solute concentration at the center are equal, i.e.

$$C_\infty(\mathbf{x}_0) - C_{\mathrm{in}}(\mathbf{x}_0).$$

With r, θ and ϕ being spherical co-ordinates the normal and tangential components of the interfacial forces for the elastic membrane in [16] are of the form

$$f_n = \gamma_{\theta\theta} + \gamma_{\phi\phi} = \beta(\lambda_\theta + \lambda_\phi - 2)$$
$$f_s = \frac{\partial \gamma_{\theta\theta}}{\partial \theta} + (\gamma_{\theta\theta} - \gamma_{\phi\phi})\cot\theta = \beta\left[\frac{\partial \lambda_\theta}{\partial \theta} + (\lambda_\theta - \lambda_\phi)\cot\theta\right] \qquad [A3]$$

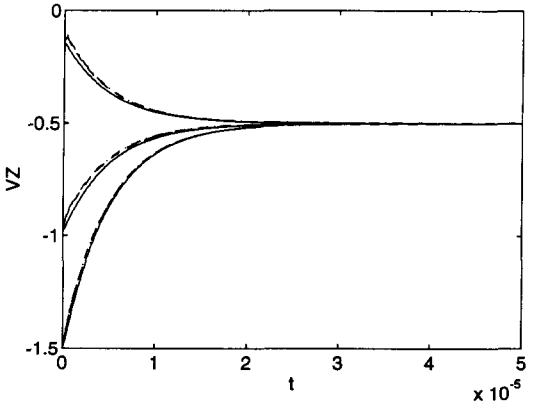

Figure A1. The evolution of the axial osmophoretic velocities of a spherical capsule. The lines correspond to six points located equidistantly on the surface along a meridional line with symmetry about the capsule center. ——, asymptotic derivation [A6]; – – –, numerical calculation with $M = 60$; – . – . –, numerical calculation with $M = 120$.

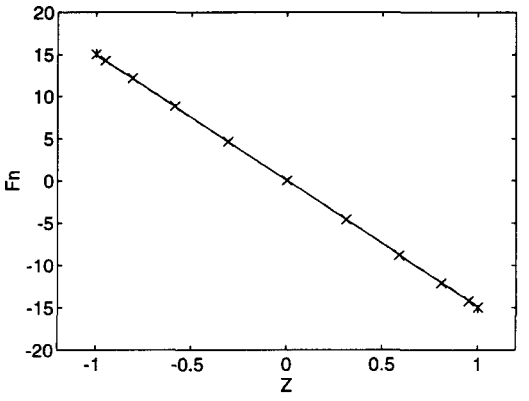

Figure A2. Interfacial normal force profile at $t = 5 \times 10^{-5}$ for the evolution described in figure A1, asymptotic calculation; —— and – – – –, numerical calculation for $M = 60$ and $M = 120$ points.

and the dynamics of the stretch ratios [6] become

$$\frac{\partial \lambda_\theta}{\partial t} = (v_r - v_{r_{os}}) + \frac{\partial v_\theta}{\partial \theta}. \quad \frac{\partial \lambda_\phi}{\partial t} = (v_r - v_{r_{os}}) + v_\theta \tan \theta \qquad [A4]$$

where $v_{r_{os}} = C_{in} - C_{out} = \Delta C$. Thus with P_j and P_j^1 being the familiar ordinary and associated Legendre polynomials, respectively, and using the expressions

$$\lambda_\theta = \sum_j L_{\theta_j} P_j(\cos\theta), \quad \lambda_\phi = \sum_j L_{\phi_j} P_j(\cos\theta), \quad \Delta C = \tfrac{3}{2} P_1(\cos\theta) \qquad [A5]$$

The Newtonian viscous surface velocity components which are of the form

$$v_r = \sum_j \frac{-2j(j+1)f_n + 3j(j+1)f_s}{(2j-1)(2j+1)(2j+3)} P_j(\cos\theta)$$

$$v_\theta = \sum_j \frac{3f_n - (2j^2+2j+3)f_s}{(2j-1)(2j+1)(2j+3)} P_j^1(\cos\theta) \qquad [A6]$$

were evaluated and used to calculate the surface axial velocity. This velocity was then compared to the numerical calculation during the early stages of the osmophoretic motion.

Figure A1 shows the dynamic axial velocity of points located on the surface calculated by the above asymptotic procedure (solid line) and the first 1000 steps of the numerical procedure for $\beta = 1 \times 10^6$ and using 60 and 120 surface points denoted by the dashed and dotted curves, respectively. The excellent agreement of the calculations of the initial transient state and the convergence to the asymptotic value is evident. Note that, although the same axial velocity is approached, all three calculations differ from Anderson's calculation (1983) since in his model interfacial tension gradients are not accounted for. Note also that the two numerical evaluations using 60 and 120 surface points are almost indistinguishable. At $t = 5 \times 10^{-5}$ the surface normal force distribution is also compared (figure A2) and the agreement between the analytical and numerical results is also remarkable.